Design, synthesis, crystal structure, biological evaluation and molecular docking studies of carbazole-arylpiperazine derivatives

Wei Xu [a,†], Junjun Huang [b,†], Binhao Shao [b], Xingjie Xu [b], Renwang Jiang [a,*], Mu Yuan [b,*]

[a] School of Pharmaceutical Sciences, Jinan University, Guangzhou 510632, China
[b] Pharmaceutical Research Center, Guangzhou Medical University, 195# Dongfengxi Road, Guangzhou 510182, China

ABSTRACT

Subtype-selective α_1-adrenoceptor (AR) antagonists display optimum therapeutic efficacies for the treatment of benign prostatic hyperplasia (BPH). In this study, we designed and synthesized novel carbazole-arylpiperazines derivatives (**1** and **2**) on the basis of the proposed pharmacophore model for α_1-AR antagonists. Structural properties were investigated using single-crystal X-ray diffraction analysis. Comparison of crystal structures with ligand-based pharmacophore models revealed that the two agents may possess antagonistic effects on α_{1D} subtype. Tissue functional assay in vitro showed that compound **2** exerted strong antagonistic activity on α_{1B}-AR (pA$_2$ 7.13) with a poor selectivity for α_{1A} and α_{1D} subtypes. Compound **1** exhibited enhanced antagonistic effect on α_{1D} subtype (pA$_2$ 7.06) and excellent selectivity for α_{1D} over α_{1B} (α_{1D}/α_{1B} ratio = 79.4). To illustrate the relationship between antagonistic activity and chemical structure, molecular docking studies were performed using the homology models of α_1 receptors. Binding mechanism indicated that small hydrophobic substituents attached to the arylpiperazine moiety were essential for rational design of α_{1D}-selective antagonists.

© 2016 Elsevier Ltd. All rights reserved.

1. Introduction

α_1-Adrenoceptors (ARs) belong to class A of the super family of G protein-coupled receptors (GPCRs) and play a key role in contracting vascular smooth and human prostate smooth muscles.[1] Based on their distinct pharmacological properties, α_1-ARs are classified into three subtypes, namely α_{1A}, α_{1B} and α_{1D}.[2,3] In the last years, subtype-selective α_1-AR antagonists were deemed to be attractive drug candidates for the treatment of benign prostatic hyperplasia (BPH) which is a common condition that severely impairs patient's health in aging males.[4,5]

Arylpiperazine derivatives exhibited extensive bioactivities including the management of BPH progression.[6] Among this kind of compounds, arylpiperazine derivatives bearing a flavone nucleus (**I**) presented in Figure 1 showed similar antagonistic properties for α_1-AR in comparison to the reference agent prazosin.[7] Although quinazolinone-arylpiperazine derivative (**II**) displayed the α_1-blocking activity less than non-selective antagonist prazosin, the compound fitted well with the ligand-based pharmacophore

model for α_1-AR antagonists which consisted of positive ionizable (PI), hydrophobic features (HY) and hydrogen bond acceptor (HBA).[8] Pyrrolidin-2-one derivative of arylpiperazine (**III**) also exhibited high affinity for the α_1-AR (pK_i = 7.30) and was further tested as α_{1A}-AR antagonist in vivo.[9] Structure–activity relationship (SAR) studies of imidazo- and indol-arylpiperazine derivatives (**IV**) validated the pharmacophore model for α_1-AR antagonists.[10] 5-arylidenehydantoin-arylpiperazine (**V**),[11] and pyridine-arylpiperazine (**VI**)[12] were also proved to possess good affinity for α_1-AR in vitro. Particularly, arylpiperazine-derived naftopidil is subtype-selective antagonist with a 15-fold selectivity for α_{1D} versus α_{1B} receptor.[13] On the other hand, carbazole derivatives displayed various biological activities, such as enzyme inhibition,[14,15] the anti-proliferation against different cancer cells lines,[16] and the 5-HT$_7$R blocking activity (**VII**).[17]

In this work, we designed novel α_1-AR antagonists that had a three-carbon linker between arylpiperazine moiety and carbazole fragments (see Fig. 2). The hypothesized pharmacophore model suggested that the hydrophobic regions are composed of carbazole group, the phenyl ring of the arylpiperazine moiety and the methoxyl substituent attached on the arylpiperazine, and the PI feature is the basic N atom on piperazine ring,[18] and the hydroxyl group is defined as hydrogen bond donor (HBD). Two carbazole-arylpiperazine derivatives were then synthesized, and fully characterized
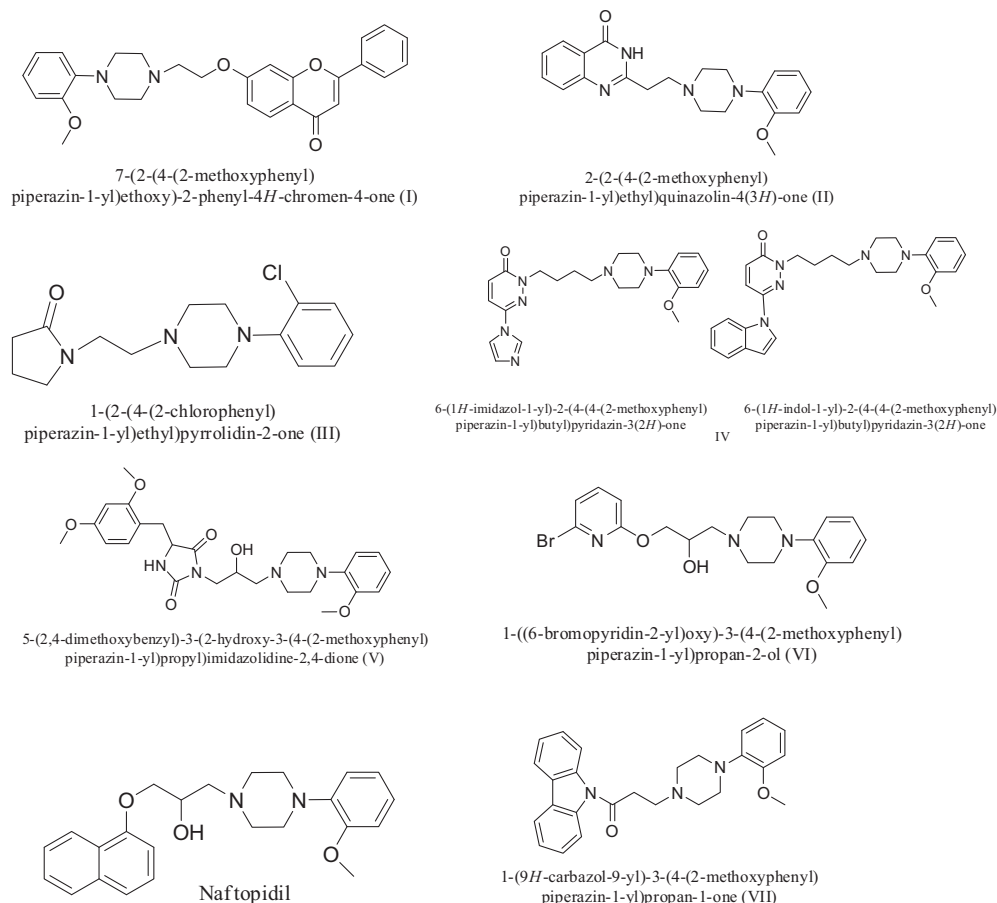
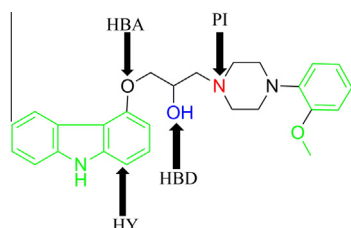**Figure 1.** Chemical structures of arylpiperazine derivatives.

Figure 2. Visualization of pharmacophoric features for novel carbazole-arylpiperazine derivatives. Colour legend: green, hydrophobic features (HY); red, positive ionizable (PI); blue, hydrogen bond donor (HBD); black, hydrogen bond acceptor (HBA).

by NMR (^{1}H and ^{13}C), elemental analysis and single crystal X-ray diffraction analysis. The antagonistic activities towards α_1-AR were evaluated using functional assays in vitro. Molecular docking studies shed light on the relationship between antagonist structures and bioactivities against α_1-AR subtypes. The work provides valuable clues for the design of subtype-selective α_1-AR antagonists.

2. Results and discussion

2.1. Chemistry

The title compounds **1** and **2** were synthesized in two steps starting from the commercially available carbazole-4-ol and 2-(chloromethyl)oxirane, as depicted in Scheme 1. The condensation of carbazole-4-ol and 2-(chloromethyl)oxirane gave the intermediate compound 4-(oxiran-2-ylmethoxy)-9H-carbazole in the presence of TEBA. 1-phenylpiperazine derivatives were prepared according to a literature method.[19] The final products (**1** and **2**) were afforded under reflux conditions, and further purified by silica gel column chromatography eluted by a mixture of ethyl acetate and petroleum ether (1/5, v/v). The structures of compounds **1** and **2** were characterized by their melting points, ^{1}H NMR, ^{13}C NMR, element analysis and single-crystal diffraction.

2.2. X-ray crystallography

Compound **1** crystallizes in the monoclinic space group Cc. The asymmetric unit contains three crystallographically independent molecules. A representative crystal structure is presented in Figure 3. The crystal data and structural refinement of **1** are presented in Table 1. The low R (5.32% for **1**, 5.17% for **2**) value in X-ray crystallography validated the synthesized structures.

As depicted in Table 2, most bond lengths are within the normal ranges, e.g., the C–C single bond in the range of 1.498(8)–1.516(8) Å, and the O–C bond lengths from 1.382(7) to 1.419(7) Å (see Table 2). The torsion angle for O(1)–C(13)–C(14)–C(15) is 62.1(7)°, −59.3(7)° and −61.9(7)° for the three independent molecules (A, B and C), respectively, which indicates that conformation A distinctly differs from another two conformers. The carbazole ring of molecular B is almost perpendicular to [C(20), C(21), C(22), C(23), C(24), C(25)] aromatic plane with a dihedral angle of 81.44(14)°, and the corresponding dihedral angles of molecular A and C are 74.23(16)° and 77.93(16)°, respectively.

The intra- and intermolecular interactions are of considerable interest in investigating the packing structures. Intramolecular O(2)–H⋯N(2) H-bond results in the formation of the pseudo-
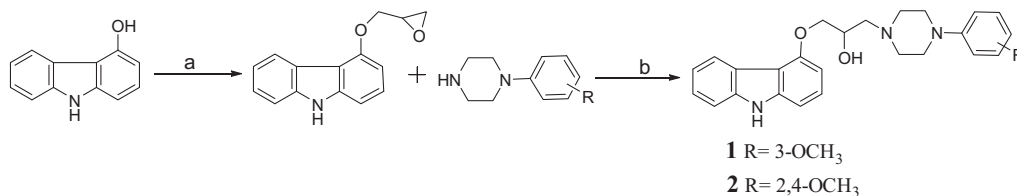
Scheme 1. Synthesis of the title compound **1** and **2**. Reagents and conditions: (a) 2-(chloromethyl)oxirane, Benzyltriethylammonium chloride (TEBA), NaOH, 70 °C; (b) CH$_3$OH, reflux.
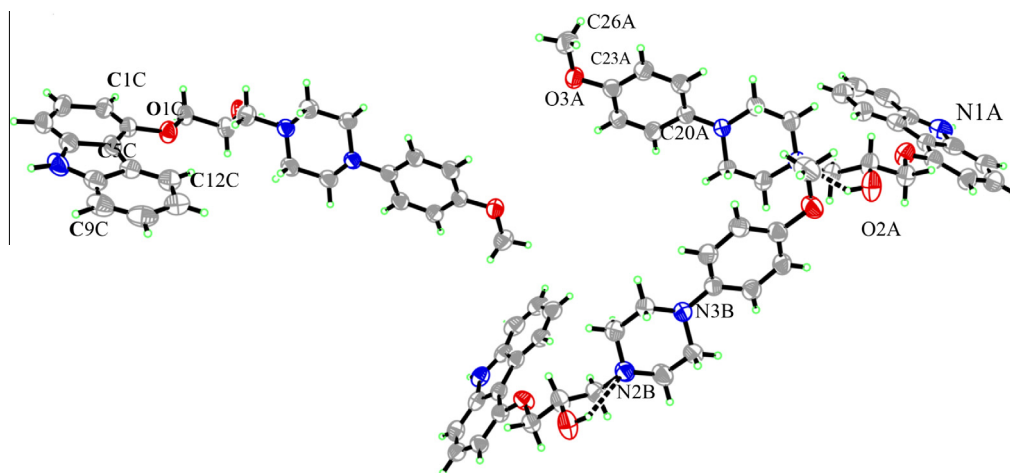

Figure 3. Crystallographic structure of **1** including three molecules in an asymmetric unit. Displacement ellipsoids are drawn at the 30% probability level, and intramolecular hydrogen bonds are presented in dashed lines.

Table 1
Crystal data and structural refinement of compounds **1** and **2**

Compound	1	2
Chemical formula	3(C$_{26}$H$_{29}$N$_3$O$_3$)	C$_{27}$H$_{31}$N$_3$O$_4$
M_r	1294.56	461.55
Temperature (K)	293(2)	293(2)
Crystal system, space group	Monoclinic, Cc	Monoclinic, $P2_1$/c
a, b, c (Å)	17.519(4), 33.882(7), 12.440(3)	8.4876(17), 11.168(2), 26.600(5)
α, β, γ (°)	90, 104.47(3), 90	90, 97.26(3), 90
V (Å^3)	7150(3)	2501.2(9)
Z	4	4
ρ_{calc} (g/cm^3)	1.203	1.226
μ (mm^{-1})	0.636	0.669
$F(000)$	2760	984
Crystal size (mm^3)	0.1 × 0.1 × 0.1	0.3 × 0.2 × 0.2
Radiation	Cu Kα (λ = 1.54178)	Cu Kα (λ = 1.54178)
θ range (°)	4.15–68.12	3.35–68.21
T_{min}/T_{max}	0.938/0.938	0.852/0.875
Reflections collected/ unique/observed	41602/12258/7537	27567/4510,/3395
R_{int}	0.0329	0.0364
Goodness-of-fit on F^2	1.071	1.093
R_1/wR_2 [I> = 2σ (I)]	0.0532/0.1504	0.0517/0.1499
R_1/wR_2 [all data]	0.0893/0.2056	0.0644/0.1640
$\Delta\rho_{max}/\Delta\rho_{min}$ (e Å^{-3})	0.30/−0.14	0.31/−0.18

five-membered rings. Intermolecular hydrogen bonds play an important role in stabilizing the packing structure (Fig. S1 and Table 3). In addition, C–H⋯π interactions reinforce the three-dimensional structure with a centroid distance of 3.472(0) Å [H⋯Cg = 2.58 Å; ∠C(10B)–H(10B)⋯Cg = 160°; Cg is the centroid of benzene ring; Symmetry code: −1/2 + x,1/2 − y, −1/2 + z].

The crystal of **2** also belongs to monoclinic system with space group $P2_1$/c, and crystal data are presented in Table 1. Ortho- and meta-methoxy stay almost coplanar with the benzene, since torsion angles of C(21)–C(22)–O(4)–C(27) and C(20)–C(25)–O(3)–C(26) are −174.5(2)° and 161.4(2)°, respectively. The dihedral angle between carbazole and benzene ring is 44.0(6)°, which is much smaller as compared to **1**. The conformational discrepancy of two X-ray structures is likely ascribed to the formation of additional intramolecular C(18)–H⋯O(3) H-bond in **2**, see Figure 4.

Intramolecular hydrogen bonds [O(2)–H⋯N(2) and C(18)–H⋯O(3)] generate non-planar five-membered and six-membered pseudo rings, respectively. As for the molecular packing (Fig. S2), two molecules form a R_1^2(5) motif via intermolecular hydrogen bonds N(1)–H⋯O(3) and N(1)–H⋯N(3). Thus, the solid-state conformation and packing structure of **2** are directly related to hydrogen bonds.

### 2.3. 3D Pharmacophore model investigations

Pharmacophore model is a benefit to designing the effective and safety antagonists at α_1-AR subtypes. Figure 5 listed the key pharmacophoric features of subtype-selective antagonists on the basis of the reported structures.[8,20] It can be seen that X-ray crystallographic structures of **1** and **2** were obviously distinguished from the reported pharmacophoric model for α_{1A}-AR antagonists, despite the distance between PI and HY1 was nearly equal. In comparison to α_{1B}-AR antagonists model, crystal structures of **1** and **2** did not match the three pharmacophoric features. This case was also confirmed by biological activities against α_1-AR that the two agents had low potency at the α_{1B} receptor (see Table 4). Interestingly, their crystal data were satisfied with the model for selective

Table 2
Selected geometric parameters of compound **1** (Å, °)

Bonds	Dist.	Bonds	Dist.	Bonds	Dist.
O(1A)–C(6A)	1.386(7)	O(1B)–C(6B)	1.377(7)	O(1C)–C(6C)	1.382(7)
O(2A)–C(14A)	1.419(7)	O(1B)–C(6B)	1.377(7)	O(1C)–C(6C)	1.382(7)
O(3A)–C(23A)	1.381(7)	O(3B)–C(23B)	1.381(6)	O(3C)–C(23C)	1.391(6)
N(1A)–C(4A)	1.374(9)	N(1B)–C(4B)	1.384(8)	N(1C)–C(4C)	1.383(8)
N(2A)–C(19A)	1.444(8)	N(2B)–C(19B)	1.458(8)	N(2C)–C(19C)	1.448(7)
C(1A)–C(2A)	1.410(9)	C(1B)–C(2B)	1.403(8)	C(1C)–C(2C)	1.402(9)
C(7A)–C(8A)	1.381(9)	C(7B)–C(8B)	1.390(8)	C(7C)–C(8C)	1.390(8)
C(13A)–C14(A)	1.498(8)	C(13B)–C14(B)	1.509(8)	C(13C)–C(14C)	1.516(8)
Angle	(°)	Angle	(°)	Angle	(°)
O(1A)–C(13A)–C(14A)	106.3(5)	O(1B)–C(13B)–C(14B)	106.1(4)	O(1C)–C(13C)–C(14C)	105.3(5)
N(1A)–C(4A)–C(5A)	108.5(7)	N(1B)–C(4B)–C(5B)	107.5(6)	N(1C)–C(4C)–C(5C)	107.2(6)
C(13A)–C(14A)–C(15A)	113.5(6)	C(13B)–C(14B)–C(15B)	115.9(5)	C(13C)–C(14C)–C(15C)	113.1(5)
O(1A)–C(13A)–C(14A)–C(15A)	62.1(7)	O(1B)–C(13B)–C(14B)–C(15B)	−59.3(7)	O(1C)–C(13C)–C(14C)–C(15C)	−62.9(7)
N(2A)–C(16A)–C(17A)–N(3A)	58.5(7)	N(2B)–C(16B)–C(17B)–N(3B)	57.2(8)	N(2C)–C(16C)–C(17C)–N(3C)	56.9(8)

Table 3
Intermolecular hydrogen bonds for compound **1** (Å, °)

D—H···A	D—H	H···A	D···A	D—H···A(°)
N(1B)—H(1B)···O(2A)^i	0.86	2.05	2.887 (7)	165
O(2A)—H(2A)···O(3B)	0.82	2.03	2.736 (4)	144
O(2B)—H(2B)···O(3A)^{ii}	0.82	2.15	2.825 (6)	140
O(2C)—H(2C)···O(3C)^{iii}	0.82	2.09	2.775 (6)	141
N(1A)—H(1AA)···O(2B)^{IV}	0.86	2.01	2.840 (8)	161

Symmetry code: (i) −1/2 + x, 1/2 + y, z (ii) x, y, 1 + z (iii) x, −y, −1/2 + z (IV) −1/2 + x, −1/2 + y, −1 + z.
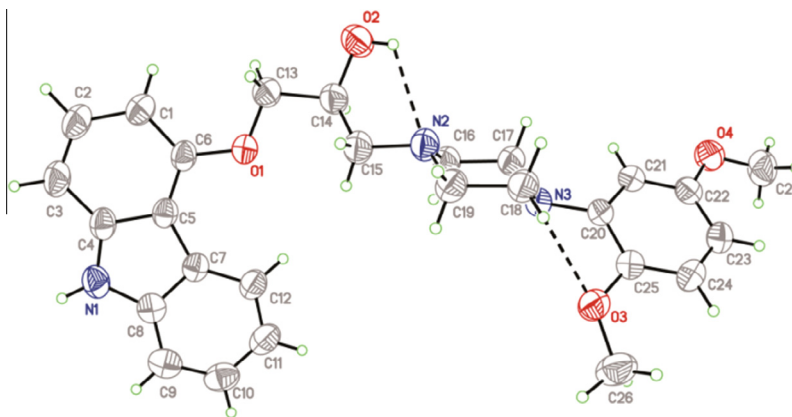
Figure 4. Crystallographic structure of **2** in an asymmetric unit. Displacement ellipsoids are drawn at the 30% probability level, and intramolecular hydrogen bonds O(2)–H···N(2) and C(18)–H···O(3) are presented in dashed lines.

α_{1D}-AR antagonists. Antagonistic effects on α_1-AR indicated that **1** displayed the highest affinity to α_{1D} in comparison with α_{1A} and α_{1B}, whereas **2** exhibited discrepancy results that the potency against α_{1B} receptor is over than that of α_{1D}.

2.4. Biological evaluation in vitro

To evaluate the subtype selectivity, the antagonistic effects of compounds **1** and **2** were characterized (Table 4). Compound **2**, which possesses two methoxyl groups at position 2 and 5, showed strong antagonistic activity on α_{1B} subtype (pA$_2$ 7.13), but had poor α_{1A}, α_{1D} subtype selectivity over α_{1B} (α_{1A}/α_{1B} ratio = 0.2, α_{1D}/α_{1B} ratio = 0.5). As compared to **2**, the 4-methoxyl-substituted derivative **1** exhibited enhanced antagonistic effect on α_{1D} subtype (pA$_2$ 7.06) and excellent selectivity concerning both α_{1D} subtype and α_{1A} subtype over α_{1B} (α_{1D}/α_{1B} ratio = 79.4, α_{1A}/α_{1B} ratio = 3.7). Moreover, the selectivity activity of **1** towards α_{1D} subtype over α_{1B} was ~5-fold higher than that of naftopidil (NAF) which was served as the positive control,[21] despite **1** had decreased potency

on α_{1D} subtype (pA$_2$ 7.06) when compared to NAF. The results of isolated tissue analysis in vitro revealed that the *para*-substituent present on the arylpiperazine moiety (**1**) led to the excellent selectivity against the α_{1D} receptor, and two methoxyl substituents located at the position *ortho* and *meta* (**2**) improved potency on α_{1B}.

2.5. Binding modes of ligand-α_1 complexes

α_1-AR is a member of the G protein-coupled receptors (GPCRs) family that are constructed by seven transmembrane (TM) helices, N- and C-terminal fragments, and intra- and extracellular loop (ECL) regions.[22] The accurate 3D structures of α_1-AR with high resolutions had not been obtained, homology-modeling strategies thus provided a viable tool for structure-based α_1-AR antagonist design.

Molecular docking studies shed light on the binding mechanism of ligand-α_1-subtype complex which can explain the observed antagonistic activities of **1** and **2**. As shown in Figure 6A, compound **1** was localized in the hydrophobic pocket involving TM I, II and
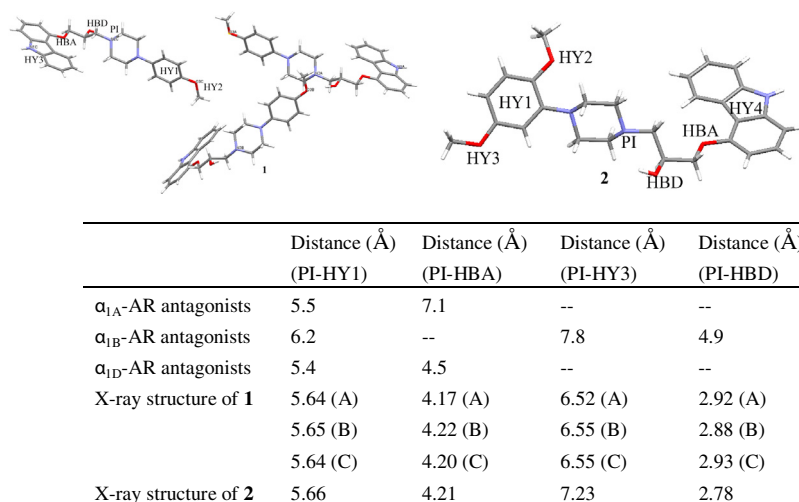
	Distance (Å) (PI-HY1)	Distance (Å) (PI-HBA)	Distance (Å) (PI-HY3)	Distance (Å) (PI-HBD)
α_{1A}-AR antagonists	5.5	7.1	--	--
α_{1B}-AR antagonists	6.2	--	7.8	4.9
α_{1D}-AR antagonists	5.4	4.5	--	--
X-ray structure of **1**	5.64 (A)	4.17 (A)	6.52 (A)	2.92 (A)
	5.65 (B)	4.22 (B)	6.55 (B)	2.88 (B)
	5.64 (C)	4.20 (C)	6.55 (C)	2.93 (C)
X-ray structure of **2**	5.66	4.21	7.23	2.78

Figure 5. Visualization of pharmacophoric features of **1** and **2** based on Barbaro's model (upper) and comparison of important distances between pharmacophoric features in reported subtype-selective α_1-AR antagonists and crystallographic structures of **1** and **2** (below).

Table 4
Functional antagonistic potency of compounds **1** and **2** (expressed as pA_2) on α_1-adrenoceptor subtypes of SD rat isolated tissues: vas deferens (α_{1A}), spleen (α_{1B}) and thoracic aorta (α_{1D})

Comp.	pA_2[a] (slope)			Selectivity ratio[b]		
	α_{1A}	α_{1B}	α_{1D}	α_{1D}/α_{1A}	α_{1D}/α_{1B}	α_{1A}/α_{1B}
1	5.73 ± 0.07 (1.01)	5.16 ± 0.11 (1.20)	7.06 ± 0.14 (1.15)	21.4	79.4	3.7
2	6.36 ± 0.10 (1.45)	7.13 ± 0.21 (0.91)	6.85 ± 0.10 (1.34)	3.1	0.5	0.2
Naftopidil[c]	7.48 ± 0.07	6.75 ± 0.11	7.93 ± 0.11	2.82	15.14	5.37

[a] pA_2 values ± SEM (n = 5–8) were calculated from Schild plots, pA_2 is the positive value of the line intercept derived through plotting log (Dr-1) versus log [antagonist].
[b] Antilog of $\triangle pA_2$.
[c] Obtained in Ref. 20.

VII. The OH group formed a hydrogen bond (2.4 Å) with the carbonyl oxygen atom of Gln177 in the ECL2 region that has been proved to be essential for GPCR activation.[23] The carbazole and benzene rings were mainly engaged in hydrophobic interactions with Phe308, Phe312 and Trp316 residues. In the **2**-α_{1A}-adrenoceptor complex, the hydroxyl group formed a H-bond with Gln177 (2.3 Å between the oxygen atom of hydroxyl group and the amide oxygen atom of Gln177). The major difference in the best poses of **1** and **2** was the localization of arylpiperazine moiety on the outer surface of TM helices.

It can be seen from Figure 6B that the carbazole rings of **1** and **2** entered into the hydrophobic region defined by Phe310, Phe311 and Phe330 residues of TM VI, and the benzene moiety contacted via hydrophobic interactions with residues Trp121, Phe334 and Tyr338 of TM VII. The OH group of **1** formed a hydrogen bond (2.9 Å) with residue Ala122 of TM III; while compound **2** established a H-bond (1.9 Å) with Val197 of ECL2, which improved the antagonistic activity against α_{1B} subtype.

Docking results showed that **1** was located in a hydrophobic pocket composed of TM III, V and VII in α_{1D} subtype (Fig. 6C). The carbazole plane was engaged in hydrophobic interactions with residues Trp112 of TM II, Phe328 and Tyr332 of TM VII, and the aromatic ring was also involved in hydrophobic interaction with the region formed by Phe304 and Phe305 of TM VI. The protonated piperazine moiety formed a weak electrostatic interaction with Glu190 of ECL2 (4.1 Å between the nitrogen atom of piperazine ring and carboxylic acid group of Glu190). For the title compound **2**, the OH group formed an H-bond to Cys186 (2.8 Å).

The binding modes were similar in antagonists **1** and **2** binding to α_{1A} receptor except that their terminal aromatic moieties presented differential localizations. The carbazole group may play an important role in the binding affinity for the α_{1A} receptor as it extended into the hydrophobic pocket. As revealed by the docking simulations, the binding poses differences between **1** and **2** was suggested to be associated with the decreased potency of **1** (pA_2 5.16) and comparatively high potency of **2** (pA_2 7.13) on the α_{1B} receptor. Recognition of Val197 of ECL2 improved the binding affinity of antagonist **2** for α_{1B}-AR. The above results discovered that favorable antagonistic activity against α_{1B} receptor could be ascribed to high hydrophobicity of the aromatic moiety and binding affinity to key residues of ECL2. Interestingly, docking modes (Fig. 6C) demonstrated that the arylpiperazine moieties of **1** and **2** as 'head' directed toward helices III, V and VII, and the carbazole group as 'tail' stayed the region near the entrance of the binding pocket of α_{1D}, which is contrary to the binding modes of the two antagonists to α_{1A} and α_{1B}-AR.

3. Conclusions

BPH is a progressive condition that severely impairs the quality of life of the aged male patients. α_1-adrenoceptor antagonists were seemed to be the most effective therapeutic strategy for BPH. In this work, two novel 1-((9H-carbazol-4-yl)oxy)-3-(4-phenylpiperazin-1-yl)propan-2-ol derivatives were synthesized and characterized by NMR and X-ray crystallographic studies. Both crystals of the title compounds **1** and **2** are monoclinic with space group Cc and $P2_1/c$, respectively. Intra- and inter-molecular hydrogen bonds play a significant role in sustaining the specific conformation and three-dimensional structures. To elucidate the relationship between structural properties and antagonistic activity, molecular
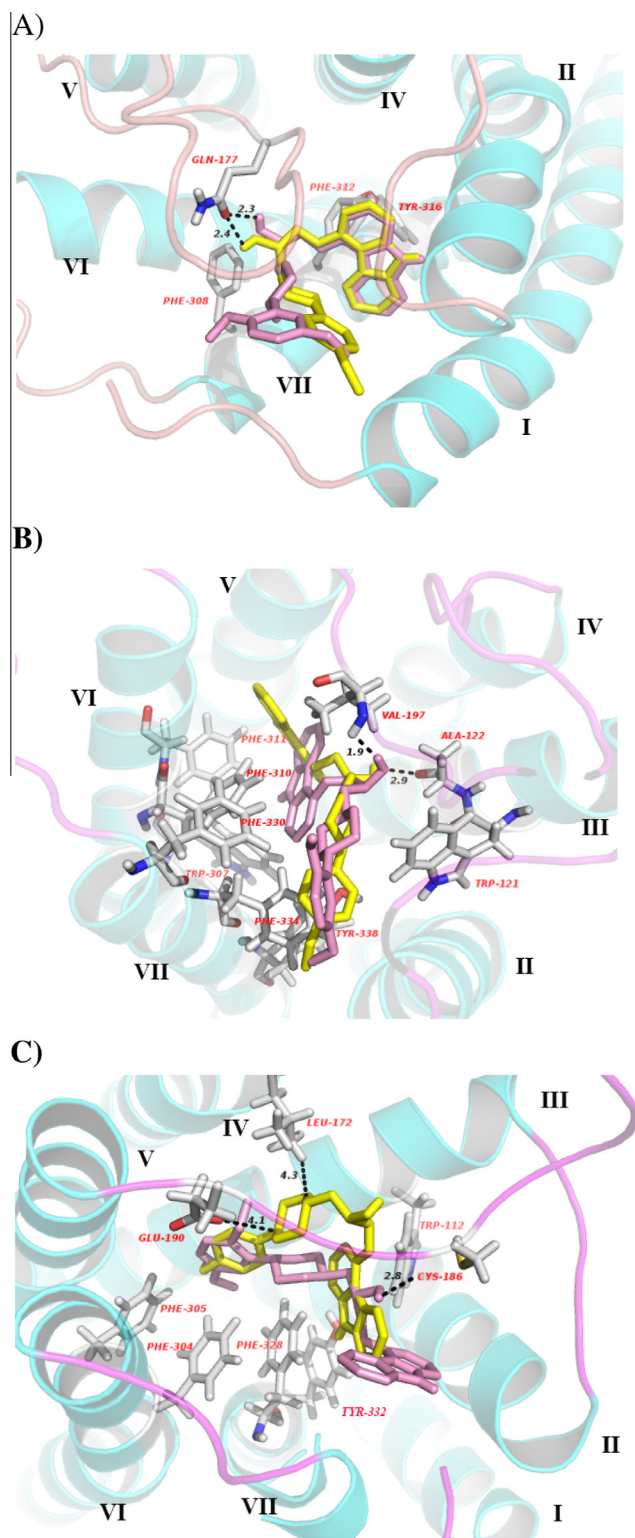
Figure 6. Selected docking poses of the α_1-AR agonists **1** (depicted in yellow) and **2** (depicted in pink) into the putative binding sites of α_{1A} (A), α_{1B} (B) and α_{1D} (C) subtypes. The two antagonists are shown in stick representation. The receptors are shown in cartoon representation with cyan alpha helices, green beta sheets and magenta loops. The seven TM helices are labeled by I, II, III, IV, V, VI and VII, respectively. Dashed lines represent the hydrogen bonds or electrostatic interactions.

docking studies using a homology model of α_1-AR was carried out. The results obtained from docking simulations showed that: (i) the

terminal carbazole group entered into the hydrophobic regions surrounded by transmembrane helices, which contributed to the improved potency against α_{1A} and α_{1B} subtypes; (ii) high hydrophobicity of aromatic moiety was benefit to the binding affinity for both α_{1A} and α_{1B}-AR, but had the opposite effect on α_{1D} subtype, and the OH group improved the potency of α_{1B} subtype through recognizing the key residues of ECL2 and (iii) introducing small hydrophobic groups to the arylpiperazine moiety was essential for rational design of α_{1D}-selective antagonists.

4. Experimental

4.1. Chemistry

All reagents and solvents were of analytical grade and commercially available. Melting points were determined on a SGW X-4 micro melting point apparatus (Shanghai Precision & Scientific Instrument Co., Ltd, Shanghai, China). NMR spectra were accomplished on a Bruker AVANCE-500 spectrometer in DMSO using TMS as the internal standard, and coupling constants (J) were quoted in Hz. Single-crystal X-ray diffraction data of compounds **1** and **2** were collected on a Rigaku RAPID II diffractometer with Cu Kα radiation ($\lambda = 1.54178$ Å). Flash column chromatography was performed with silica gel (Qing Dao Ocean Chemical Factory, 300–400 mesh).

4.1.1. Synthesis of 1-((9H-carbazol-4-yl)oxy)-3-(4-(4-methoxy-phenyl)piperazin-1-yl)propan-2-ol (1)

A mixture of 4-(oxiran-2-ylmethoxy)-9H-carbazole (100 mg, 0.44 mmol) and 1-(4-methoxyphenyl)piperazine (126.8 mg, 0.66 mmol) in methanol (10 ml) was refluxed for 2 h. When the reaction was complete, as indicated by TLC, the solvent was evaporated under reduced pressure. The residue was purified by silica gel column chromatography (petroleum ether/ethyl acetate = 5/1, v/v) to give the desired compound **1** (119.5 mg, 63% yield) as a white solid. mp 202–204 °C. ^{1}H NMR (500 MHz, DMSO-d_6) δ 11.23 (s, 1H), 8.25 (d, $J = 7.7$ Hz, 1H), 7.44 (d, $J = 8.0$ Hz, 1H), 7.33 (t, $J = 7.3$ Hz, 1H), 7.28 (t, $J = 8.0$ Hz, 1H), 7.14 (t, $J = 7.4$ Hz, 1H), 7.07 (d, $J = 8.0$ Hz, 1H), 6.86 (d, $J = 9.1$ Hz, 2H), 6.79 (d, $J = 9.1$ Hz, 2H), 6.69 (d, $J = 7.9$ Hz, 1H), 5.02 (d, $J = 3.4$ Hz, 1H), 4.37–4.00 (m, 3H), 3.66 (s, 3H), 3.00 (t, $J = 4.4$ Hz, 4H), 2.77–2.53 (m, 6H).^{13}C NMR (126 MHz, DMSO-d_6) δ 155.52, 153.32, 145.96, 141.61, 139.41, 126.99, 125.02, 123.03, 122.25, 119.05, 117.76, 114.72, 112.10, 110.85, 104.32, 100.96, 71.29, 67.31, 61.84, 55.66, 54.17, 50.16. Anal. Calcd for $C_{26}H_{29}N_3O_3$: C, 72.30; H, 6.72; N, 9.73. Found: C, 72.23; H, 6.74; N, 9.59.

4.1.2. Synthesis of 1-((9H-carbazol-4-yl)oxy)-3-(4-(2,5-dimetho-xyphenyl)piperazin-1-yl)propan-2-ol (2)

A mixture of 4-(oxiran-2-ylmethoxy)-9H-carbazole (100 mg, 0.44 mmol) and 1-(2,5-dimethoxyphenyl)piperazine (146.6 mg, 0.66 mmol) in methanol (10 ml) was refluxed for 2 h. When the reaction was complete, as indicated by TLC, the mixture was concentrated under reduced pressure, and purified by silica gel column chromatography eluting with petroleum ether/ethyl acetate (5/1, v/v) to afford compound **2** (101.5 mg, 50% yield). mp 162–164 °C. ^{1}H NMR (500 MHz, DMSO-d_6) δ 11.24 (s, 1H), 8.26 (d, $J = 7.8$ Hz, 1H), 7.45 (d, $J = 8.0$ Hz, 1H), 7.37–7.32 (m, 1H), 7.30 (t, $J = 8.0$ Hz, 1H), 7.15 (t, $J = 7.4$ Hz, 1H), 7.07 (d, $J = 8.0$ Hz, 1H), 6.81 (d, $J = 8.7$ Hz, 1H), 6.70 (d, $J = 7.9$ Hz, 1H), 6.46 (dd, $J = 8.7$, 2.9 Hz, 1H), 6.43 (d, $J = 2.9$ Hz, 1H), 5.01 (d, $J = 4.5$ Hz, 1H), 4.57–3.93 (m, 3H), 3.71 (s, 3H), 3.67 (s, 3H), 2.98 (s, 4H), 2.78–2.53 (m, 6H). ^{13}C NMR (126 MHz, DMSO-d_6) δ 155.00, 153.75, 146.16, 142.34, 141.08, 138.88, 126.47, 124.50, 122.51, 121.73, 118.52, 112.98, 111.57, 110.32, 105.44, 105.08, 103.78, 100.43, 70.79, 66.73,

```
        1           11          21          31          41
alpha 1D SGEDNRSSAG  EPGSAGAGGD  VN-GTAAVGG  LVVSAQGVGV  GVFLAAFILM
3SN6_R   - - - - - - - - - -  - - - - - - - - - -  - - - - - - - VGM  GIvMSIIVLa
2R4R_A   - - - - - - - - - -  - - - - - - - - - -  - - - - - - - VGM  GIvMSIIVLa
2RH1_A   - - - - - - - - - -  - - - - - - - - - -  - - - - - - - VGM  GIvMSIIVLa
4XEE_A   - - DDDaTSTS  EsdTAGpNSD  LDvNTdiySk  VLVTA- - - - -  - IYLAIFVVg

        51          61          71          81          91
alpha 1D AVAGNLLVIL  SVACNRHLQT  V- - - TNYFIV  NLAVADLLLS  ATVLPFSATM
3SN6_R   ivfGNVLVIt  AIAkfERLQT  V- - - TNYFIT  SLAcADLVMG  IAVVPFGAAh
2R4R_A   ivfGNVLVIt  AIAkfERLQT  V- - - TNYFIT  SLAcADLVMG  IAVVPFGAAh
2RH1_A   ivfGNVLVIt  AIAkfERLQT  V- - - TNYFIT  SLAcADLVMG  IAVVPFGAAh
4XEE_A   TV-GNsVTLF  TLArKKsLQS  LqstVHYhLg  SLALSDLLII  IIAMP- - - -V

        101         111         121         131         141
alpha 1D EVLGF- - - - -  - WAFGRAFCD  VWAAVDVLCC  TASILSLCTI  SVDRYVGVRH
3SN6_R   iLtkt- - - - -  - WTFGNfWCE  fWTSIDVLCv  TASIeTLCVI  AVDRYfAIts
2R4R_A   iLMkM- - - - -  - WTFGNfWCE  fWTSIDVLCv  TASIeTLCVI  AVDRYfAIts
2RH1_A   iLMkM- - - - -  - WTFGNfWCE  fWTSIDVLCv  TASIeTLCVI  AVDRYfAIts
4XEE_A   ELyNFiwvhh  pWAFGdAgCr  gYyfLrdaCt  yATaLNVASL  SVERYLAIcH

        151         161         171         181         191
alpha 1D SLKYPAIMTE  RKAAAILALL  WVVALVVSVG  PL- - LGW- - -  - - K- - - -EPV
3SN6_R   pFKYqSLLTK  NKArVIIIMV  WIVSgLTSfl  Plq-MhWyra  thQ- - - -Eal
2R4R_A   pFKYqSLLTK  NKArVIIIMV  WIVSgLTSfl  Plq-MhWyra  thQ- - - -Eal
2RH1_A   pFKYqSLLTK  NKArVIIIMV  WIVSgLTSfl  Plq-MhWyra  thQ- - - -Eal
4XEE_A   pFKakTLMSR  sRTkkFISal  WLASaLLAlp  mLftMGI- - -  - - QnrsaDgT

        201         211         221         231         241
alpha 1D P- - PDERFCG  - ITEEAGYAV  - - - FSSVCSF  YLPMAVIVVM  YCRVYVVARS
3SN6_R   ncyaEEtcCd  - FftNqAYAl  - - - aSSIvSF  YVPLVIMVfV  YsRVFqeA- -
2R4R_A   ncyaNEtcCd  - FftNqAYAl  - - - aSSIvSF  YVPLVIMVfV  YsRVFqeA- -
2RH1_A   ncyaEEtcCd  - FftNqAYAl  - - - aSSIvSF  YVPLVIMVfV  YsRVFqeAKr
4XEE_A   h- - PgglvCt  pIVDtAtvkV  viqvNTfmSF  IFPMIVIsIL  nt- - - VIANK

        251         261         271         281         291
alpha 1D TTRSLEAGVK  RERGKASEVV  LRIHCRG-AA  TGADG- -AHG  MRSAKGHTFR
3SN6_R   - - - - - - - - K  RQIqKiDKse  gRFHvQNISq  VeqDGrtGHG  LR- - - - - - -R
2R4R_A   - - - - - - - - K  RQIqKiDKse  gRFHvQNISq  VeqDGrtGHG  LR- - - - - - -R
2RH1_A   qINiFE- - -  - - - - - - - - - -  - - - - - - - - - -  - - - - - - - - - -  - - - - - - - - - -
4XEE_A   ITvmVHqAA-  - EQGRVctV-  - - - - - -G-Th  NGIEh- -S- -  - - - - - - -TF-

        301         311         321         331         341
alpha 1D SSLSVRLLKF  S-REKKAAKT  LAIVVGVFVL  CWFPFFFVLP  LGSLFPQLKP
3SN6_R   SS- - - - - -KF  cIKEhKAIKT  LGIIMGTFTL  CWLPFFIVni  VhvIqdNLir
2R4R_A   SS- - - - - -KF  cIKEhKAIKT  LGIIMGTFTL  CWLPFFIVni  VhvIqdNLir
2RH1_A   - - - - - - - - - -  - - - - - - - - - -  - - - - - - - - - -  - - - - - - - - - -  - - - - - - - - - -
4XEE_A   -NMTIEpgRv  Q-aIRhGVIV  LraVViAFVV  CWLPYhvrrl  MfcyIsDeQw

        351         361         371         381         391
alpha 1D SEGVFKVIFW  - - - - - -LGY  FNSCVNPLIY  PCSSREFKRA  FLRLLRCQCR
3SN6_R   KE-VYiLLnW  - - - - - -IGY  vNSgfNPLIY  -CrSpDFRiA  FqELL- - -CI
2R4R_A   KE-VYiLLnW  - - - - - -IGY  vNSgfNPLIY  -CrSpDFRiA  FqELL- - -CI
2RH1_A   - - - - - - - - - -  - - - - - - - - - -  - - - - - - - - - -  - - - - - - - - - -  - - - - - - - - - -
4XEE_A   TtfLFdfyhY  fymItnaLfY  aSSAINPILY  nIvSaNFRQV  FLstLaCICp

        401
alpha 1D RRRRRRPLWR
3SN6_R   RR- - - - - - -
2R4R_A   RR- - - - - - -
2RH1_A   - - - - - - - - - -
4XEE_A   gwRHRR- - - -
```

Figure 7. Amino acid sequence alignments of 3SN6, 2R4R, 2RH1, 4XEE with Alpha 1D.

61.41, 55.88, 55.13, 53.79, 49.95. Anal. Calcd for $C_{27}H_{31}N_3O_4$: C, 70.20; H, 6.72; N, 9.10. Found: C, 70.33; H, 6.70; N, 9.03.

4.2. X-ray crystallography

Suitable crystals were obtained by slowly evaporating a mixture of dichloromethane and n-hexane solution at ambient temperature. Colorless crystals were mounted on a thin glass fiber in a random orientation. The data were collected by a R-AXIS RAPID II diffractometer equipped with graphite-monochromatic Cu Kα radiation ($\lambda = 1.54178$ Å) by using a ω scan mode. The structures were solved by direct methods using Olex2 software,[24] and the non-hydrogen atoms were located from the trial structure and then refined anisotropically with SHELXL-2014[25] using a full-matrix least squares procedure based on F^2. The weighted R factor, wR and goodness-of-fit S values were obtained based on F^2. The hydrogen atom positions were fixed geometrically at the calculated distances and allowed to ride on their parent atoms. Crystallographic data for the structure reported in this Letter have been deposited at the Cambridge Crystallographic Data Center and allocated with the deposition numbers: CCDC 1032470 and 1028230 for compounds **1** and **2**, respectively.

4.3. Tissue functional assays in vitro

Isolated thoracic aorta rings, spleen and vas deferens of adult mature rats (Sprague–Dawley strain, 200–350 g) were used to test antagonistic activities of investigated compounds (**1** and **2**) for α_{1D}, α_{1B}, α_{1A} subtype, respectively. These tissues were dissected and placed into Krebs–Henseleit solution (NaCl 119 mM, KCl 4.7 mM, $CaCl_2$ 1.9 mM, $MgSO_4$ 1.2 mM, KH_2PO_4 1.2 mM, $NaHCO_3$ 25 mM, glucose 11 mM, EDTA 0.05 mM, pH 7.4) at temperature 37 °C and pH 7.4 with constant oxygenation (O_2/CO_2, 19:1).[20]

The thoracic aorta rings (approximately 4-mm long) were subjected to an optimal tension and allowed to equilibrate for 1.5 h. Then, noradrenaline (NA 1 mM) were added into stimulate three times, and washed until the contractile response had become constant. The tissues were incubated with antagonists for 0.5 h. Concentration–response curves of NA were measured at an interval of 1 h in the absence and presence of antagonists. To block alpha2- and beta-adrenoceptors, the experiments were conducted in the continuous presence of yohimbine (0.1 mM) and propranolol (1 mM). The other two tissues were performed the similar experimental protocols.

Concentration–response curves were analyzed using GraphPad Prism 5.0 software (GraphPad Software Inc., San Diego, CA, USA).[26] As the reference of the maximal NA effect (E_{max} = 100%) obtained before incubation with the tested compounds, contractile responses to antagonists are expressed as a percentage. The data are the means ± SEM of at least 5 separate experiments, and the final pA_2 values are obtained from the linear regression of Schild plot.[27]

4.4. Homology modeling and molecular docking

The amino acidic sequences of the human α_{1A}, α_{1B}, α_{1D} receptor were retrieved from SwissProt database (entry code P35348, ADA1A_HUMAN; P35368, ADA1B_HUMAN; P25100, ADA1D_HUMAN). The homology models of α_{1A} and α_{1B} receptors were generated due to our previously reported methods.[6,28] To construct α_{1D} model, BlastP of α_{1D} sequence against Protein Data Bank (PDB) in combination with UCSF Chimera 1.10.2 package was performed to search a suitable template.[29] The protein structures (PDB: 3SN6, 2R4R, 2RH1, 4XEE) with high E values, scores, and wide coverages were selected as best suitable templates (Fig. 7), and the sequence identity with alpha 1D was 41.80% for 3SN6, 41.80% for 2R4R, 38.31% for 2RH1 and 25.63% for 4XEE, respectively. The homology model of α_{1D} subtype was generated by using the program Modeller 9.10 (all parameters were left at the default values).[30] The model was then submitted to be energy optimization by using CHARMMing program. Structural evaluation and stereochemical analyses were performed using PROCHECK, PROVE, CRYST and Ramchandran plot.[31] PyMOL software was employed for checking and validating protein structures after model refinement.

Conformation A in the crystallographic asymmetric unit of compound **1** was subject to molecular docking studies based on the comparison of the geometrical parameters between calculated model and crystal structure. Stable conformation of compound **2** extracted from the crystal structures was saved in mol2 format. The preparation of the pdbqt files was done by standard procedure using AutoDock Tools 1.5.6.[32] The docking procedures were performed in AutoDock Vina using the default scorring function.[33] The binding site was identified according to previous studies.[6] Exhaustiveness was set to 100, and number of output conformations was set to 20. The searching seed was random. The calculated geometries were ranked in terms of free energy of binding and the best poses were selected for further analysis.

Acknowledgments

A. Supplementary data

Supplementary data associated with this article can be found, in the online version, at http://dx.doi.org/10.1016/j.bmc.2016.09.010.

These data include MOL files and InChiKeys of the most important compounds described in this article.

References and notes

1. Sarswat, A.; Kumar, R.; Kumar, L.; Lal, N.; Sharma, S.; Prabhakar, Y. S.; Pandey, S. K.; Lal, J.; Verma, V.; Jain, A.; Maikhuri, J. P.; Dalela, D.; Gupta, G.; Sharma, V. L. *J. Med. Chem.* **2011**, *54*, 302.
2. Meyer, M. D.; Altenbach, R. J.; Bai, H.; Basha, F. Z.; Carroll, W. A.; Kerwin, J. F.; Lebold, S. A., Jr.; Lee, E.; Pratt, J. K.; Sippy, K. B.; Tietje, K.; Wendt, M. D.; Brune, M. E.; Buckner, S. A.; Hancock, A. A.; Drizin, I. *J. Med. Chem.* **2001**, *44*, 1971.
3. Nanda, K.; Naruganahalli, K. S.; Gupta, S.; Malhotra, S.; Tiwari, A.; Hegde, L. G.; Jain, S.; Sinha, N.; Gupta, J. B.; Chugh, A.; Anand, N.; Ray, A. *Eur. J. Pharmacol.* **2009**, *607*, 213.
4. Kinsella, G. K.; Rozas, I.; Watson, G. W. *J. Med. Chem.* **2006**, *49*, 501.
5. Ventura, S.; Oliver, V.; White, C. W.; Xie, J. H.; Haynes, J. M.; Exintaris, B. *Br. J. Pharmacol.* **2011**, *163*, 891.
6. Xu, W.; Huang, J. J.; Shao, B. H.; Xu, X. J.; Jiang, R. W.; Yuan, M. *Molecules* **2015**, *20*, 19674.
7. Jin, Y.; Wang, X. B.; Kong, L. Y. *Bioorg. Med. Chem. Lett.* **2011**, *21*, 909.
8. Abou-Seri, S. M.; Abouzid, K.; Abou El Ella, D. A. *Eur. J. Med. Chem.* **2011**, *46*, 647.
9. Zaręba, P.; Dudek, M.; Lustyk, K.; Siwek, A.; Starowicz, G.; Bednarski, M.; Nowiński, L.; Raźny, K.; Sapa, J.; Malawska, B.; Kulig, K. *Bioorg. Med. Chem.* **2015**, *23*, 2104.
10. Strappaghetti, G.; Mastrini, L.; Lucacchini, A. *Bioorg. Med. Chem.* **2008**, *18*, 5140.
11. Handzlik, J.; Szymańska, E.; Wójcik, R.; Dela, A.; Jastrzębska-Więsek, M.; Karolak-Wojciechowska, J.; Fruziński, A.; Siwek, A.; Filipek, B.; Kieć-Kononowicz, K. *Bioorg. Med. Chem.* **2012**, *20*, 4245.
12. Handzlik, J.; Szymańska, E.; Wójcik, R.; Dela, A.; Jastrzębska-Więsek, M.; Karolak-Wojciechowska, J.; Fruziński, A.; Zylewski, M. *Med. Chem.* **2014**, *10*, 144.
13. Castiglione, F.; Benigni, F.; Briganti, A.; Salonia, A.; Villa, L.; Nini, A.; Di Trapani, E.; Capitanio, U.; Hedlund, P.; Montorsi, F. *Curr. Med. Res. Opin.* **2014**, *30*, 719.
14. Zimmermann, K.; Sang, X.; Mastalerz, H. A. *Bioorg. Med. Chem. Lett.* **2015**, *25*, 2809.
15. Akrami, H.; Mirjalili, B. F.; Khoobi, M.; Moradi, A.; Nadri, H.; Emami, S.; Foroumadi, A.; Vosooghi, M.; Shafiee, A. *Arch. Pharm. (Weinheim)* **2015**, *348*, 366.
16. Chen, Y.; Tang, C.; Wu, Y. *Org. Biomol. Chem.* **2015**, *13*, 6773.
17. Kim, Y.; Yeom, M.; Tae, J.; Rhim, H.; Choo, H. *Eur. J. Med. Chem.* **2016**, *110*, 302.
18. MacDougall, I. J.; Griffith, R. *J. Mol. Graph. Model* **2006**, *25*, 146.
19. Kossakowski, J.; Pakosinska-Parys, M.; Struga, M.; Dybala, I.; Koziol, A. E.; Collu, D.; Loddo, R. *Molecules* **2009**, *14*, 5189.
20. Handzlik, J.; Bojarski, A. J.; Satała, G. *Eur. J. Med. Chem.* **2014**, *78*, 324.
21. Huang, J.; He, F.; Huang, M.; Liu, X.; Xiong, Y.; Huang, Y.; Zhu, L.; Yang, Y.; Xu, X.; Yuan, M. *Eur. J. Med. Chem.* **2015**, *96*, 83.
22. Goldfeld, D. A.; Zhu, K.; Beuming, T.; Friesner, R. A. *Proc. Natl. Acad. Sci. U.S.A.* **2011**, *108*, 8275.
23. de Graaf, C.; Foata, N.; Engkvist, O. *Proteins* **2008**, *71*, 599.
24. Dolomanov, O. V.; Bourhis, L. J.; Gildea, R. J. *J. Appl. Crystallogr.* **2009**, *42*, 339.
25. Kratzert, D.; Holstein, J. J.; Krossing, I. *J. Appl. Crystallogr.* **2015**, *48*, 933.
26. Handzlik, J.; Maciag, D.; Kubacka, M.; Mogilski, S.; Filipek, B.; Stadnicka, K.; Kieć-Kononowicz, K. *Bioorg. Med. Chem.* **2008**, *16*, 5982.
27. Nirogi, R. V.; Bandyala, T. R.; Reballi, V. *J. Enzyme Inhib.* **2015**, *30*, 85.
28. Xu, W.; Shao, B. H.; Xu, X. J.; Yuan, M. *J. Mol. Struct.* **2016**, *1106*, 485.
29. Nettles, J. H.; Stanton, R. A.; Broyde, J.; Amblard, F.; Zhang, H.; Zhou, L.; Shi, J.; McBrayer, T. R.; Whitaker, T.; Coats, S. J.; Kohler, J. J.; Schinazi, R. F. *J. Med. Chem.* **2014**, *57*, 10031.
30. Yrjölä, S.; Parkkari, T.; Navia-Paldanius, D.; Laitinen, T.; Adusei-Mensah, F.; Savinainen, J. R.; Laitinen, J. T.; Poso, A.; Alexander, A.; Penman, J.; Stott, L.; Anskat, M.; Irving, A. J.; Nevalainen, T. J. *Eur. J. Med. Chem.* **2016**, *107*, 119.
31. Sashidhara, K. V.; Avula, S. R.; Doharey, P. K.; Singh, L. R.; Balaramnavar, V. M.; Gupta, J.; Misra-Bhattacharya, S.; Rathaur, S.; Saxena, A. K.; Saxena, J. K. *Eur. J. Med. Chem.* **2015**, *103*, 418.
32. Luo, W.; Chen, Y.; Wang, T.; Hong, C.; Chang, L. P.; Chang, C. C.; Yang, Y. C.; Xie, S. Q.; Wang, C. J. *Bioorg. Med. Chem.* **2016**, *24*, 672.
33. Trott, O.; Olson, A. J. *J. Comput. Chem.* **2010**, *31*, 455.